

Route to hyperchaos in quadratic optomechanics

Lina Halef¹ and Itay Shomroni^{1,*}

¹*Racah Institute of Physics, The Hebrew University of Jerusalem, Jerusalem 9190401, Israel*

(Dated: October 15th, 2024)

Hyperchaos is a qualitatively stronger form of chaos, in which several degrees of freedom contribute simultaneously to exponential divergence of small changes. A hyperchaotic dynamical system is therefore even more unpredictable than a chaotic one, and has a higher fractal dimension. While hyperchaos has been studied extensively over the last decades, only a few experimental systems are known to exhibit hyperchaotic dynamics. Here we introduce hyperchaos in the context of cavity optomechanics, in which light inside an optical resonator interacts with a suspended oscillating mass. We show that hyperchaos can arise in optomechanical systems with quadratic coupling that operate in the resolved-sideband regime by applying a far off-resonance, blue-detuned pump, and is well within reach of current experiments. We compute the two positive Lyapunov exponents, characteristic of hyperchaos, and independently verify the correlation dimension. As systems designed for high-precision measurements, optomechanical systems enable direct measurement of all four dynamical variables and therefore the full reconstruction of the hyperchaotic attractor. Our results may contribute to better understanding of nonlinear systems and the chaos-hyperchaos transition, and allow the study of hyperchaos in the quantum regime.

I. INTRODUCTION

Ultraprecise optical measurements of mechanical motion underly pivotal technologies such as gravitational wave detectors [1] and atomic [2] and magnetic [3] force microscopes. Light also carries momentum which can be used to manipulate mechanical objects, e.g. in optical tweezers [4]. Cavity optomechanics [5] studies these interactions at the fundamental level, employing a wide range of engineered mechanical oscillators, in a setup where the oscillator is coupled to light enclosed in a high-quality optical cavity. The main focus is the ensuing quantum dynamics, with the aim to develop novel quantum technologies [6], search for dark matter [7], or address questions regarding quantum theory at the macroscopic scale [8].

While most works focus on the linear regime of small oscillations, the optomechanical interaction is fundamentally nonlinear and can lead to rich dynamics. The existence of multiple period-1 limit cycles (sustained oscillations under a continuous optical drive) was studied in [9] and explored experimentally in [10, 11]. As the nonlinearity increases (e.g., by increasing the drive), a cascade of period-doubling bifurcations finally lead to chaos [12]. Indeed, an early observation in optomechanics was that of chaotic mechanical motion [13]. Sustained oscillations and chaos in optomechanics were further analyzed in various regimes [14–20] including in the quantum regime [12, 21, 22]. Experimental work is scant, however, and often relies on other nonlinearities such as thermal effects or Duffing nonlinearity [23–26].

In this work we introduce a novel and rare feature in the dynamics of optomechanical systems: hyperchaos. A hallmark of chaos is sensitivity to initial conditions.

In most dynamical systems, however, this sensitivity is dominated by a single dimension in phase space. In other words, an infinitesimal volume on a chaotic attractor will tend to stretch at an exponential rate along a single dimension transverse to the orbit. While ubiquitous, this form of chaos is the lowest stage in a hierarchy of chaotic dynamics [27]—since it is possible that the expansion occur along multiple dimensions. Such ‘hyperchaotic’ behavior [28] has been studied theoretically over the last decades [29–34]. Despite this interest, only a handful of experiments demonstrated hyperchaotic dynamics, among which are electronic circuits [35], an NMR system [36], a semiconductor [37], a certain chemical reaction [38], lasers with delayed feedback [39, 40], and optical solitons [41]. Unfortunately, with the exception of electronic circuits, in all these experiments both the governing equations and the dimension of phase space are unknown. Moreover, most dynamical variables cannot be measured in the experiment, and the structure of phase space must be inferred indirectly using techniques which are susceptible to noise, and greatly exaggerate its dimensionality [42]. This severely limits the insight that can be gained by studying these systems. Hyperchaos has also been recently predicted in the polarization of vertical-cavity surface-emitting lasers [43], semiconductor superlattices [44], hydromagnetic convection [45] and coupled two-level systems [46]—all of which also suffer from lack of full experimental access to the dynamical variables.

In contrast, in optomechanical systems all degrees of freedom can be measured with high precision. In addition, the phase space has only four dimensions, the minimum required for hyperchaos, making it considerably simpler than the preceding examples. Another attractive advantage is the ability to explore hyperchaos in the quantum regime. We identify regimes where hyperchaotic dynamics occur in optomechanical systems *with quadratic coupling* [47–52]. Specifically, hyperchaos

* itay.shomroni@mail.huji.ac.il

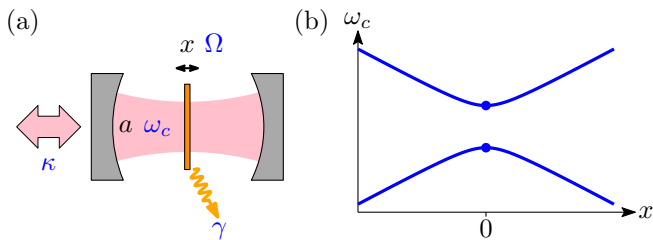


FIG. 1. Quadratic optomechanical coupling. (a) Membrane-in-the-middle system. A thin dielectric membrane with natural frequency Ω oscillates with displacement x within the mode a of a Fabry-Perot cavity, shifting the cavity resonance frequency ω_c . The cavity decay rate through the input/output port is κ and the oscillator decay rate is γ . (b) Dependence of ω_c on x . Only part of the full mode spectrum is shown, with two widely separated branches, originating from the hybridization of the modes of the two half-cavities. Quadratic coupling occurs at $x = 0$.

arises when the mechanical frequency exceeds the cavity decay rate, i.e., the resolved sideband regime.

II. THE SYSTEM

Optomechanical systems [5] are based on a parametric coupling between light inside an optical cavity and an integrated mechanical oscillator. The oscillator displacement x shifts the resonance frequency ω_c of the cavity by changing the optical path of the light, which in turn exerts a force on the oscillator through radiation pressure. In quadratic optomechanical systems, some form of symmetry nullifies the first-order dependence of ω_c on x , leading to a frequency shift proportional to x^2 [47–52]. The canonical example is the so-called membrane-in-the-middle (MIM) system [53–55] shown in Fig. 1(a). A thin (usually tens of nanometers) semitransparent membrane is placed inside a Fabry-Perot cavity. If placed at the node or antinode of the modal intensity distribution, two coupled normal modes appear, as shown in Fig. 1(b). The coupling is strong in typical systems due to the relatively low reflectance of the membrane. As a consequence, the mode separation is larger than any other rate in the system, such that only one mode participates in the dynamics (the adiabatic approximation [56]).

The dynamics are then governed by the Hamiltonian

$$H = \frac{p^2}{2m} + \frac{1}{2}m\Omega^2x^2 + \hbar(\omega_c + Gx^2)a^\dagger a. \quad (1)$$

The first two terms describe the free evolution of the oscillator, of mass m and frequency Ω , and momentum p conjugate to x . The third term describes the cavity field mode, characterized by the photon creation and annihilation operators a^\dagger, a respectively. The coupling constant $G = \frac{1}{2}\partial^2\omega_c/\partial x^2$ determines the strength of the interaction. Note that positive or negative G can be selected, depending on which of the two modes we choose to work with [Fig. 1(b)].

The Hamiltonian (1) is formulated quantum-mechanically as is standard in cavity optomechanics. It contains Planck’s constant \hbar due to our use of photons. We assume that the cavity is pumped with a strong coherent laser drive of frequency $\omega_l = \omega_c + \Delta$ and amplitude E . The cavity and oscillator energy decay rates are κ and γ , respectively. By scaling time and κ, γ, Δ by the mechanical frequency Ω and defining the dimensionless quantities [57]

$$\tilde{a} = \frac{\Omega}{2E}a, \quad \tilde{x} = \sqrt{\frac{G}{\Omega}}x, \quad \tilde{p} = \sqrt{\frac{G}{m^2\Omega^3}}p, \quad P = \frac{8\hbar GE^2}{m\Omega^4} \quad (2)$$

we obtain the classical equations of motion in a frame rotating with the drive frequency ω_l (removing the tildes from x, p, a for clarity)

$$\dot{x} = p \quad (3a)$$

$$\dot{p} = -(1 + P|a|^2)x - \gamma p \quad (3b)$$

$$\dot{a} = i(\Delta - x^2)a - \frac{\kappa}{2}a + \frac{1}{2}. \quad (3c)$$

Equations (3) are nonlinear and cannot be solved analytically. There are four parameters: the cavity and oscillator decay rates κ, γ are typically fixed by the experimental system, while the pump P , which sets the strength of the nonlinearity, and the detuning Δ can be tuned easily by adjusting the pumping laser. The oscillator typically has a very high quality factor, $\gamma \ll 1$.

It is well known that both linear and quadratic coupling optomechanical systems exhibit phenomena such as multistability [9], period-doubling bifurcations, and chaos [12, 16, 19]. We note that since a is complex, there are four equations in real variables, which is the minimum required for hyperchaos.

Equation (3b) shows that the quadratic coupling shifts the mechanical frequency, proportional to the light intensity $|a|^2$. If $P < 0$, the frequency of the oscillator may become negative, leading to unbounded motion. Here we focus exclusively on $P > 0$, corresponding to the upper branch of Fig. 1(b) where ω_c has a minimum at $x = 0$. In this case the system has a single fixed point (where all time derivatives are zero), $x = p = 0, a = 1/(\kappa - 2i\Delta)$. This fixed point is stable for all parameter values, hence transitions to self-sustained oscillations (limit cycles), and later to chaos, cannot occur through Hopf bifurcations as in other optomechanical systems [12, 16], and need to be excited externally, i.e. by setting the initial condition of the oscillator. In an experiment, the oscillator can be initialized in the desired state by first applying a pump tuned to the lower branch of Fig. 1(b), where $P < 0$ and other fixed points exist, or by mechanical excitation.

Equations (3), with the addition of linear x coupling, have been analyzed in previous works. When $\kappa \gg 1$, the cavity field can be adiabatically eliminated, resulting in an effective potential for the oscillator [58, 59]. Self-sustained oscillations and ordinary chaotic motion were studied in [14, 15] for $\kappa \sim 1$ and small detunings $|\Delta| \sim 1$.

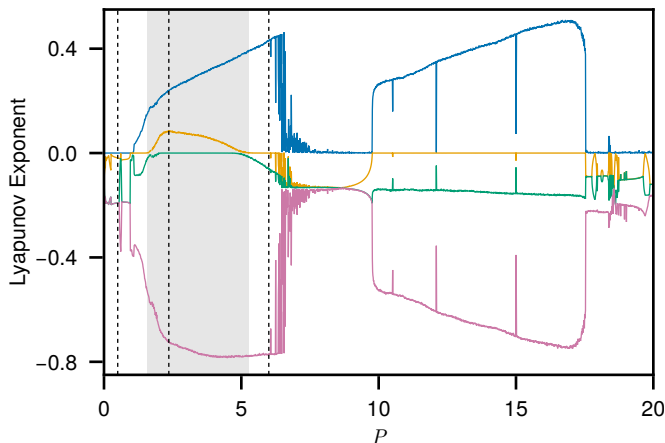


FIG. 2. The Lyapunov exponents of a system with $\kappa = 0.4$, $\gamma = 10^{-3}$, and $\Delta = 15.5$, for varying P . The initial condition is $(x, p, a) = (4, 4, 0)$. The shaded region highlights the range with two positive LEs, indicating hyperchaos.

III. CHAOS AND HYPERCHAOS

A trajectory in phase space of a dynamical system is characterized by its spectrum of Lyapunov exponents (LEs), the number of which equals the dimension of the phase space [60]. The LEs quantify the divergence of infinitesimally nearby trajectories, hence the sensitivity to initial conditions. A single positive LE means that nearby trajectories separate exponentially fast, and is sufficient to classify the motion as chaotic. If more than one LE is positive, however, then exponential separation can occur along mutually independent directions, which indicates higher complexity of motion and is termed ‘hyperchaos’ [28].

Figure 2 shows the four LEs of the system (3) with $\kappa = 0.4$, $\gamma = 10^{-3}$, $\Delta = 15.5$, and varying P . The initial condition is $(x, p, a) = (4, 4, 0)$. In the region $1.6 < P < 5$ two LEs are positive, indicating hyperchaotic behavior in this parameter range. Furthermore for $9.8 < P < 17.5$ only one LE is positive, i.e., the motion is merely chaotic. At $P \simeq 2.36$ the second largest LE λ_2 attains its maximal value, and the two positive LEs are $(\lambda_1, \lambda_2) \simeq (0.240, 0.085)$. For a more complete picture, Fig. 3 shows three trajectories, for the cases of a limit cycle, chaotic, and hyperchaotic dynamics, categorized by the Lyapunov spectrum and indicated by dashed lines in Fig. 2. All the trajectories cover the same time interval and contain the same number of points. In all cases, the dynamics of the light field a are more complex than that of the oscillator [see also the insets of Fig. 3(d–f)]. Below we discuss discerning hyperchaotic from chaotic dynamics quantitatively, but here we note that the hyperchaotic trajectory is more spread out than the chaotic one, despite the latter having larger nonlinearity P .

It is noteworthy that optical cavities are rarely used with such large detunings, $\Delta/\kappa \approx 40$. In the absence of the oscillator, at this detuning only $\sim 1.5 \times 10^{-4}$ of the

maximal energy (for resonant pumping) would be stored in the cavity. Nevertheless, as Fig. 3 shows, for sufficiently high power (and appropriate initial conditions) both the oscillator and field coordinates approach their on-resonance values.

We investigate the occurrence of hyperchaos for different parameters in Fig. 4. Figure 4(a) fixes $\kappa = 0.4$ and shows the two largest LEs $\lambda_{1,2}$ as a function of Δ and P . The effect of the cavity linewidth κ is shown in Fig. 4(b). Here, we check for hyperchaos by taking the largest value attained by $\lambda_{1,2}$ for any $\Delta \in [0, 20]$. Figure 4(b) shows that hyperchaos occurs for $\kappa \lesssim 0.6$, i.e. in the resolved sideband regime of optomechanics. This regime has been relatively underexplored in nonlinear optomechanics. A recent work [19] explored chaos in this regime, though of optomechanics with linear coupling.

We now turn to the important question of how to distinguish hyperchaos from chaos in an experiment. While chaotic motion is easy to distinguish from a non-chaotic one, for example by observing the power spectral density of the cavity output light [13] [see Fig. 3(d–f)], verifying hyperchaotic motion is not as straightforward. One conventional approach is to estimate the LEs from an experimentally acquired time series [61, 62]. In most experiments, only a subset of phase space can be measured directly, but the LEs (and other invariants) can be evaluated by embedding the data in higher-dimensional spaces using time delays. However, this approach may not be optimal for LEs other than the maximal due to measurement noise [42].

In contrast, a remarkable advantage of optomechanical systems is experimental access to all four dynamical variables. The quadratures of the intracavity field a can be measured directly via heterodyne detection of the cavity output, and the position x and momentum p of the oscillator can be measured using a weak probe laser of a different wavelength, where linear coupling is dominant. Hence the LEs can be calculated more accurately, with no need for time-delay embedding.

An attractor is also classified by its fractal dimension D , measuring its degree of self-similarity. For an ordinary chaotic attractor $2 < D < 3$, while for hyperchaos $D > 3$. We use the standard method to estimate D of simulated trajectories using the correlation dimension method of Grassberger and Proccacia [63]. This estimate is independent of the underlying equations and can therefore corroborate the existence of hyperchaos. Figure 5 shows the estimated fractal dimension D of a hyperchaotic system with $\kappa = 0.4$, $\gamma = 0.007$, $\Delta = 15.5$ and varying P (see Appendix B for numerical details). We have chosen a larger mechanical decay rate in order to reduce the transient time of the dynamics, $\sim \gamma^{-1}$. There is an excellent agreement between the hyperchaotic region with two positive LEs and $D > 3$, and the chaotic region with $D \lesssim 3$. To the best of our knowledge, estimation of D for an experimentally-relevant hyperchaotic system was not carried out before. This is an interesting avenue of further research, given the difficulty in accurate numerical

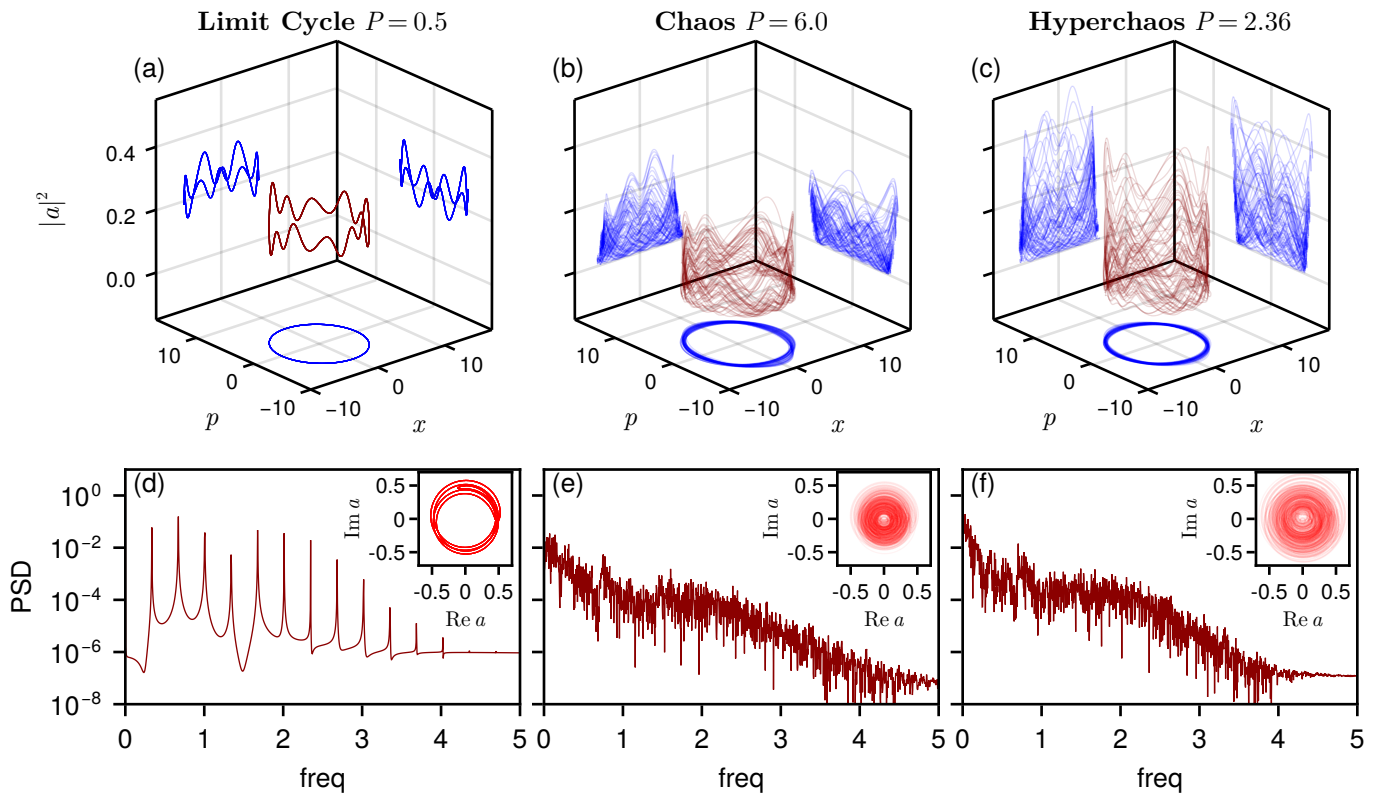


FIG. 3. Phase space trajectories of a system with the same parameters as Fig. 2, for cases of a limit cycle (left column), chaos (middle column) and hyperchaos (right column). These parameters are also indicated with the dashed lines in Fig. 2. Panels (a–c) show the trajectories using the variables x , p , $|a|^2$, along with the projections of each variable pair. Panels (d–f) show the power spectral densities of the intracavity field a . The insets show the trajectories of the quadratures of a .

simulations of the dynamics.

IV. EXPERIMENTAL RELEVANCE

The main challenge in observing hyperchaos in an experiment is the optical power needed to achieve the required value of P . Too high pumping power will lead to deleterious effects such as excess heating that will hinder the measurement. In addition, the cavity mirrors should have the same reflectivity, to avoid dissipative coupling [64, 65].

For a MIM system, the coupling rate $G = \frac{1}{2}\partial^2\omega_c/\partial x^2$ is evaluated from the cavity response to the position x , given by $\omega_c(x) = 2\nu_{\text{FSR}} \arccos[r_d \cos(2kx)]$, where $k = 2\pi/\lambda$ is the wavenumber for light of wavelength λ , $\nu_{\text{FSR}} = c/2L$ is the free spectral range of a cavity with length L , and r_d the amplitude reflectivity of the membrane [54]. Pure quadratic coupling occurs when $2kx = \pi n$ for integer n , where

$$\frac{\partial^2\omega_c}{\partial x^2} = 8k^2\nu_{\text{FSR}} \frac{r_d}{\sqrt{1-r_d^2}}. \quad (4)$$

The pumping amplitude E can be written as $\sqrt{\kappa_{\text{ex}}}a_{\text{in}}$ where $|a_{\text{in}}|^2$ is the input photon flux and κ_{ex} is the cavity

input coupling rate. We assume $\kappa_{\text{ex}} = \kappa$ for simplicity. Collecting all the parameters, we can express the required incident power on the cavity for a given P as

$$\frac{\text{incident power}}{P} = \frac{\Omega^4\lambda mL}{32\pi\kappa_{\text{ex}}} \sqrt{\frac{1-r_d^2}{r_d^2}} \quad (5)$$

For example, Ref. 66 reports a membrane with $\Omega = 2\pi \times 101.9$ kHz, $m = 3 \times 10^{-12}$ kg, and $r_d = 0.58$ at $\lambda = 532$ nm. Setting $L = 30$ mm and $\kappa = 0.4\Omega$ yields a ‘modest’ cavity finesse of 20,000 and only 1 mW of pump power to achieve $P = 2.36$ required for observation of hyperchaos. For these parameters, $x = 1$ corresponds to 8 times the r.m.s of thermal fluctuations of the oscillator at room temperature. Optomechanical systems using levitated nanospheres [67, 68] are also attractive, due to the small mass $m \sim 10^{-17}$ kg and mechanical frequencies $\Omega/2\pi \sim 10$ –100 kHz set by an external potential. We conclude that observation of hyperchaotic optomechanical motion is very feasible with current systems.

V. CONCLUSION

We have shown that hyperchaos exists in quadratic optomechanics and is observable with current experimen-

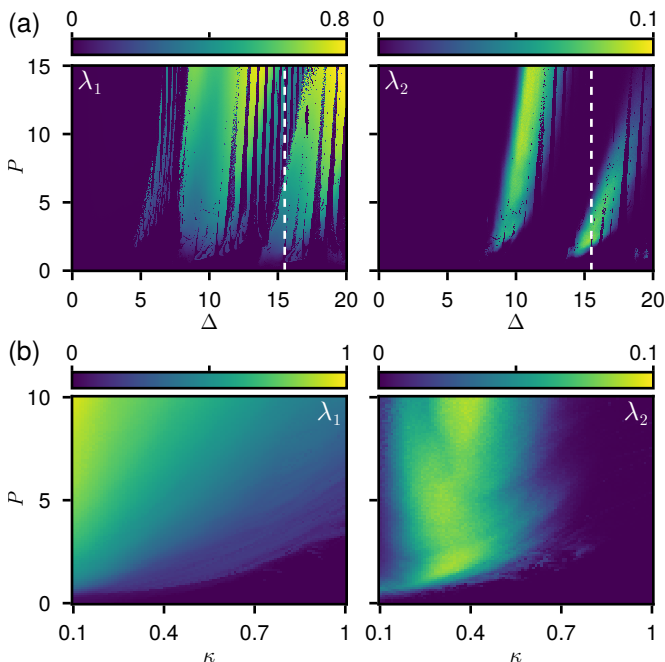


FIG. 4. Occurrence of hyperchaos for various system parameters. (a) Values of the maximal LE λ_1 and second LE λ_2 vs. the detuning Δ and pump power P , with fixed cavity decay rate $\kappa = 0.4$. The dashed white lines correspond to Fig. 2(a). (b) Effect of the linewidth κ for different pumping powers P , where the colormaps show, each independently, the largest values of λ_1, λ_2 obtained in the range $\Delta \in [0, 20]$ for a given (κ, P) . The other parameters are $\gamma = 10^{-3}$ and initial condition $(x, p, a) = (4, 4, 0)$.

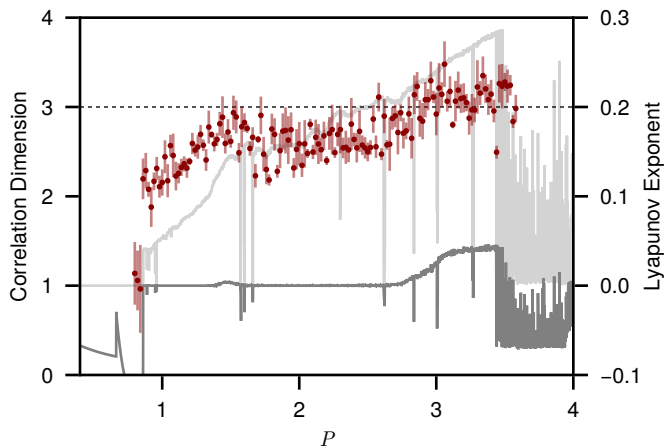


FIG. 5. Estimation of the fractal dimension, using the correlation dimension. System parameters are $\kappa = 0.4$, $\gamma = 0.007$, and $\Delta = 15.5$. The data (red, left axis) is overlaid on the first two Lyapunov exponents (right axis). There is excellent correlation between the second LE (dark gray) becoming positive, indicating hyperchaos, and the dimension exceeding 3, indicated by the dashed line. The dimension is obtained using the Grassberger-Procaccia method. Error bars indicate the standard error of a linear fit to the scaling curve, see Appendix B. Note the increase of D in the small hyperchaotic region near $P = 1.5$.

tal systems. It is important to note that while we focused here on pure quadratic coupling, our calculations show that hyperchaos exists also in the presence of additional linear coupling. Furthermore, while we presented a system with the minimal required dimensionality for hyperchaos, this can be extended by incorporating additional optical and mechanical modes. Another interesting prospect is hyperchaos in the quantum regime, which is routinely accessible in optomechanical systems.

The chaos-hyperchaos transition remains an active field of research [32, 33, 69] with implications to a wide range of scientific fields [70–72]. Optomechanics can serve as an ideal experimental platform for the study of these phenomena.

Data Availability. The code and data used to produce the plots within this paper are available from the corresponding author upon reasonable request.

ACKNOWLEDGMENTS

We thank Omri Gat, Snir Gazit, and Nils J. Engelsen for fruitful discussions. This work was supported by the Israel Science Foundation Grant No. 695/22. L.H. acknowledges support from the Kaete Klausner Scholarship.

Appendix A: Equations of motion

For computation, Eqs. (3) can be recast using real variables. Setting $a_x = \text{Re } a$ and $a_p = \text{Im } a$ we have

$$\dot{x} = p \quad (\text{A1a})$$

$$\dot{p} = -x - P(a_x^2 + a_p^2)x - \gamma p \quad (\text{A1b})$$

$$\dot{a}_x = -\Delta a_p + x^2 a_p - \frac{\kappa}{2} a_x + \frac{1}{2} \quad (\text{A1c})$$

$$\dot{a}_p = \Delta a_x - x^2 a_x - \frac{\kappa}{2} a_p \quad (\text{A1d})$$

The corresponding Jacobian is

$$J = \begin{pmatrix} 0 & 1 & 0 & 0 \\ -P(a_x^2 + a_p^2) - 1 & -\gamma & -2Pxa_x & -2Pxa_p \\ 2xa_p & 0 & -\kappa/2 & -\Delta + x^2 \\ -2xa_x & 0 & \Delta - x^2 & -\kappa/2 \end{pmatrix}. \quad (\text{A2})$$

The fixed points of the system are found by setting the time derivatives in (3) to zero, giving

$$0 = p \quad (\text{A3a})$$

$$0 = x(1 + P|a|^2) \quad (\text{A3b})$$

$$\frac{1}{2} = \left[-i(\Delta - x^2) + \frac{\kappa}{2} \right] a \quad (\text{A3c})$$

if $P > 0$, we have $x = 0$ from Eq. (A3b), and the only fixed point is $x = p = 0$, $a = (\kappa - 2i\Delta)^{-1}$. It can be shown that the real part of the eigenvalues of the fixed

point Jacobian are always negative (for $P > 0$ and $\gamma < 2$) making this fixed point stable.

For $P < 0$ there are additional fixed points with $x \neq 0$ and $|a|^2 = -1/P$. Taking the square magnitude of Eq. (A3c) we have

$$(\Delta - x^2)^2 = \frac{-P - \kappa^2}{4}. \quad (\text{A4})$$

These fixed points exist if the right-hand side is positive. We then define $\mu \equiv \sqrt{-P - \kappa^2}$ and

$$x = \pm \sqrt{\Delta \pm \frac{\mu}{2}} \quad (\text{A5})$$

which exist when the radicand is positive. For all fixed points with $x \neq 0$, we have

$$a = \frac{1}{\kappa - i\mu} = -\frac{\kappa}{P} - i\frac{\mu}{P} = \frac{1}{\sqrt{-P}} e^{i\phi}, \quad (\text{A6})$$

where $\cos \phi = \kappa/\sqrt{-P}$.

Appendix B: Numerical Details

Convergence of the Lyapunov exponents. Numerical simulations were done in Julia using the ChaosTools package [73]. The values of the LEs were verified in Python using the lyapunov package and by hand-coding Benettin's algorithm [74, 75]. Figure 6 shows the convergence of the computed LEs as a function of the number of steps.

Correlation dimension. For the computation of the correlation dimension in Fig. 5, we integrated the dynamical equations for each P using the DifferentialEquations Julia package. To obtain the extremely high accuracy needed, we employed Feagin's 14th order explicit Runge-Kutta solver using arbitrary precision arithmetic, setting the absolute (relative) accuracy to 10^{-70} (10^{-67}). The system was propagated from $t = 0$ to $t = 550$, discarding data up to $t = 200$ to eliminate transients. The trajectories were then standardized. The correlation sum $C(\epsilon)$ was calculated using the FractalDimensions Julia package [76], the interpoint distance ϵ ranging from one

octave above to two octaves below its minimal/maximal values respectively. A Theiler window of 70 time units was used, but other choices do not modify the results substantially. The trajectories were simulated with a time step $dt = 0.001$. To calculate $C(\epsilon)$ for each trajectory, we divided it into ten interleaving trajectories with $dt = 0.01$ and averaged $C(\epsilon)$ over these. This was done to further reduce temporal correlations but again does not impact the results. The correlation dimension was estimated by a simple linear least-squares fit of $\log C$ vs. $\log \epsilon$, starting from values of $C(\epsilon)$ resulting from at least 100,000 pairs, and its error by the standard error of this estimate. Though it has been pointed out that such estimates are not completely accurate [77], we find it gives

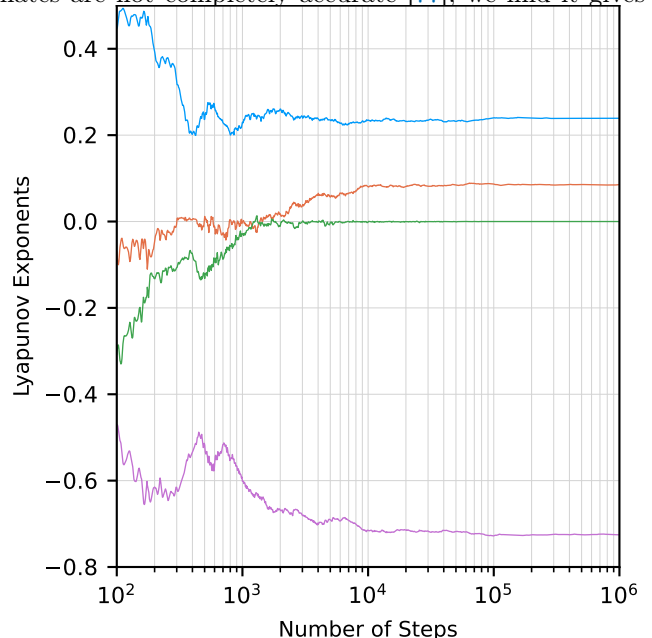


FIG. 6. Convergence of the Lyapunov exponents. Calculated with parameters $\{P, \Delta, \kappa, \gamma\} = \{2.36, 15.5, 0.4, 0.001\}$ and initial condition $(x, p, a) = (4, 4, 0)$. The time step between orthogonalizations is $\Delta t = 0.1$.

good agreement in our case. A more involved method to compute the scaling region and correlation dimension was also employed [78], and gave similar results.

[1] The LIGO Scientific Collaboration *et al.*, Advanced LIGO, *Classical and Quantum Gravity* **32**, 074001 (2015).
 [2] F. J. Giessibl, Advances in atomic force microscopy, *Reviews of Modern Physics* **75**, 949 (2003).
 [3] D. Rugar, R. Budakian, H. J. Mamin, and B. W. Chui, Single spin detection by magnetic resonance force microscopy, *Nature* **430**, 329 (2004).
 [4] A. Ashkin, Acceleration and Trapping of Particles by Radiation Pressure, *Physical Review Letters* **24**, 156 (1970).

[5] M. Aspelmeyer, T. J. Kippenberg, and F. Marquardt, Cavity optomechanics, *Reviews of Modern Physics* **86**, 1391 (2014).
 [6] S. Barzanjeh, A. Xuereb, S. Gröblacher, M. Paternostro, C. A. Regal, and E. M. Weig, Optomechanics for quantum technologies, *Nature Physics* **18**, 15 (2022).
 [7] D. Carney, G. Krnjaic, D. C. Moore, C. A. Regal, G. Afek, S. Bhave, B. Brubaker, T. Corbitt, J. Cripe, N. Crisosto, A. Geraci, S. Ghosh, J. G. E. Harris, A. Hook, E. W. Kolb, J. Kunjummen, R. F. Lang, T. Li,

- T. Lin, Z. Liu, J. Lykken, L. Magrini, J. Manley, N. Matsumoto, A. Monte, F. Monteiro, T. Purdy, C. J. Riedel, R. Singh, S. Singh, K. Sinha, J. M. Taylor, J. Qin, D. J. Wilson, and Y. Zhao, Mechanical quantum sensing in the search for dark matter, *6*, 024002 (2021).
- [8] A. J. Leggett, Testing the limits of quantum mechanics: motivation, state of play, prospects, *Journal of Physics: Condensed Matter* **14**, R415 (2002).
- [9] F. Marquardt, J. G. E. Harris, and S. M. Girvin, Dynamical Multistability Induced by Radiation Pressure in High-Finesse Micromechanical Optical Cavities, *Physical Review Letters* **96**, 103901 (2006).
- [10] A. G. Krause, J. T. Hill, M. Ludwig, A. H. Safavi-Naeini, J. Chan, F. Marquardt, and O. Painter, Nonlinear Radiation Pressure Dynamics in an Optomechanical Crystal, *Physical Review Letters* **115**, 233601 (2015).
- [11] F. M. Buters, H. J. Eerkens, J. Heck, M. J. Weaver, B. Pepper, S. de Man, and D. Bouwmeester, Experimental exploration of the optomechanical attractor diagram and its dynamics, *Physical Review A* **92**, 013811 (2015).
- [12] L. Bakemeier, A. Alvermann, and H. Fehske, Route to Chaos in Optomechanics, *Physical Review Letters* **114**, 013601 (2015).
- [13] T. Carmon, M. C. Cross, and K. J. Vahala, Chaotic Quivering of Micron-Scaled On-Chip Resonators Excited by Centrifugal Optical Pressure, *Physical Review Letters* **98**, 167203 (2007).
- [14] L. Zhang and H.-Y. Kong, Self-sustained oscillation and harmonic generation in optomechanical systems with quadratic couplings, *Physical Review A* **89**, 023847 (2014).
- [15] L. Zhang, F. Ji, X. Zhang, and W. Zhang, Photon-phonon parametric oscillation induced by quadratic coupling in an optomechanical resonator, *Journal of Physics B: Atomic, Molecular and Optical Physics* **50**, 145501 (2017).
- [16] C. Wurl, A. Alvermann, and H. Fehske, Symmetry-breaking oscillations in membrane optomechanics, *Physical Review A* **94**, 063860 (2016).
- [17] J. Mumford, D. H. J. O'Dell, and J. Larson, Dicke-type phase transition in a multimode optomechanical system, *Annalen der Physik* **527**, 115 (2015).
- [18] X.-Y. Lü, H. Jing, J.-Y. Ma, and Y. Wu, \mathcal{PT} -Symmetry-Breaking Chaos in Optomechanics, *Physical Review Letters* **114**, 253601 (2015).
- [19] T. F. Roque, F. Marquardt, and O. M. Yevtushenko, Nonlinear dynamics of weakly dissipative optomechanical systems, *New Journal of Physics* **22**, 013049 (2020).
- [20] D.-W. Zhang, C. You, and X.-Y. Lü, Intermittent chaos in cavity optomechanics, *Physical Review A* **101**, 053851 (2020).
- [21] M. Ludwig, B. Kubala, and F. Marquardt, The optomechanical instability in the quantum regime, *New Journal of Physics* **10**, 095013 (2008).
- [22] C. Schulz, A. Alvermann, L. Bakemeier, and H. Fehske, Optomechanical multistability in the quantum regime, *Europhysics Letters* **113**, 64002 (2016).
- [23] F. Monifi, J. Zhang, c. K. Özdemir, B. Peng, Y.-x. Liu, F. Bo, F. Nori, and L. Yang, Optomechanically induced stochastic resonance and chaos transfer between optical fields, *Nature Photonics* **10**, 399 (2016).
- [24] D. Navarro-Urrios, N. E. Capuj, M. F. Colombano, P. D. García, M. Sledzinska, F. Alzina, A. Griol, A. Martínez, and C. M. Sotomayor-Torres, Nonlinear dynamics and chaos in an optomechanical beam, *Nature Communications* **8**, 14965 (2017).
- [25] J. Wu, S.-W. Huang, Y. Huang, H. Zhou, J. Yang, J.-M. Liu, M. Yu, G. Lo, D.-L. Kwong, S. Duan, and C. Wei Wong, Mesoscopic chaos mediated by Drude electron-hole plasma in silicon optomechanical oscillators, *Nature Communications* **8**, 15570 (2017).
- [26] G. Madiot, F. Correia, S. Barbay, and R. Braive, Bichromatic synchronized chaos in driven coupled electro-optomechanical nanoresonators, *Physical Review A* **104**, 023525 (2021).
- [27] O. E. Rossler, The Chaotic Hierarchy, *Zeitschrift für Naturforschung A* **38**, 788 (1983).
- [28] O. E. Rossler, An equation for hyperchaos, *Physics Letters A* **71**, 155 (1979).
- [29] T. Kapitaniak and W. H. Steeb, Transition to hyperchaos in coupled generalized van der Pol equations, *Physics Letters A* **152**, 33 (1991).
- [30] M. A. Harrison and Y.-C. Lai, Route to high-dimensional chaos, *Physical Review E* **59**, R3799 (1999).
- [31] T. Kapitaniak, Y. Maistrenko, and S. Popovych, Chaos-hyperchaos transition, *Physical Review E* **62**, 1972 (2000).
- [32] A. N. Pavlov, O. N. Pavlova, Y. K. Mohammad, and J. Kurths, Characterization of the chaos-hyperchaos transition based on return times, *Physical Review E* **91**, 022921 (2015).
- [33] R.-H. Du, S.-X. Qu, and Y.-C. Lai, Transition to high-dimensional chaos in nonsmooth dynamical systems, *Physical Review E* **98**, 052212 (2018).
- [34] S. Leo Kingston, M. Balcerzak, S. K. Dana, and T. Kapitaniak, Transition to hyperchaos and rare large-intensity pulses in Zeeman laser, *Chaos: An Interdisciplinary Journal of Nonlinear Science* **33**, 023128 (2023).
- [35] T. Matsumoto, L. Chua, and K. Kobayashi, Hyperchaos: Laboratory experiment and numerical confirmation, *IEEE Transactions on Circuits and Systems* **33**, 1143 (1986).
- [36] R. Stoop and P. F. Meier, Evaluation of Lyapunov exponents and scaling functions from time series, *JOSA B* **5**, 1037 (1988).
- [37] R. Stoop, J. Peinke, J. Parisi, B. Röhrlich, and R. P. Huebener, A p-Ge semiconductor experiment showing chaos and hyperchaos, *Physica D: Nonlinear Phenomena* **35**, 425 (1989).
- [38] M. Eiswirth, T. M. Krueel, G. Ertl, and F. W. Schneider, Hyperchaos in a chemical reaction, *Chemical Physics Letters* **193**, 305 (1992).
- [39] I. Fischer, O. Hess, W. Elsässer, and E. Göbel, High-Dimensional Chaotic Dynamics of an External Cavity Semiconductor Laser, *Physical Review Letters* **73**, 2188 (1994).
- [40] Y. Deng, Z.-F. Fan, B.-B. Zhao, X.-G. Wang, S. Zhao, J. Wu, F. Grillot, and C. Wang, Mid-infrared hyperchaos of interband cascade lasers, *Light: Science & Applications* **11**, 7 (2022).
- [41] A. S. Bir, S. V. Grishin, O. I. Moskalenko, A. N. Pavlov, M. O. Zhuravlev, and D. O. Ruiz, Experimental Observation of Ultrashort Hyperchaotic Dark Multisoliton Complexes in a Magnonic Active Ring Resonator, *Physical Review Letters* **125**, 083903 (2020).
- [42] H. D. I. Abarbanel, R. Brown, J. J. Sidorowich, and L. S. Tsimring, The analysis of observed chaotic data in physical systems, *Reviews of Modern Physics* **65**, 1331 (1993).

- [43] C. Bonatto, Hyperchaotic Dynamics for Light Polarization in a Laser Diode, *Physical Review Letters* **120**, 163902 (2018).
- [44] E. Mompó, M. Carretero, and L. Bonilla, Designing Hyperchaos and Intermittency in Semiconductor Superlattices, *Physical Review Letters* **127**, 096601 (2021).
- [45] W. M. Macek and M. Strumik, Hyperchaotic Intermittent Convection in a Magnetized Viscous Fluid, *Physical Review Letters* **112**, 074502 (2014).
- [46] A. V. Andreev, A. G. Balanov, T. M. Fromhold, M. T. Greenaway, A. E. Hramov, W. Li, V. V. Makarov, and A. M. Zagoskin, Emergence and control of complex behaviors in driven systems of interacting qubits with dissipation, *npj Quantum Information* **7**, 1 (2021).
- [47] J. C. Sankey, C. Yang, B. M. Zwickl, A. M. Jayich, and J. G. E. Harris, Strong and tunable nonlinear optomechanical coupling in a low-loss system, *Nature Physics* **6**, 707 (2010).
- [48] T. K. Paraiso, M. Kalaei, L. Zang, H. Pfeifer, F. Marquardt, and O. Painter, Position-Squared Coupling in a Tunable Photonic Crystal Optomechanical Cavity, *Physical Review X* **5**, 041024 (2015).
- [49] H. Kaviani, C. Healey, M. Wu, R. Ghobadi, A. Hryciw, and P. E. Barclay, Nonlinear optomechanical paddle nanocavities, *Optica* **2**, 271 (2015).
- [50] R. Burgwal, J. d. Pino, and E. Verhagen, Comparing nonlinear optomechanical coupling in membrane-in-the-middle and single-cavity systems, *New Journal of Physics* **22**, 113006 (2020).
- [51] N. P. Bullier, A. Pontin, and P. F. Barker, Quadratic optomechanical cooling of a cavity-levitated nanosphere, *Physical Review Research* **3**, L032022 (2021).
- [52] R. Burgwal and E. Verhagen, Enhanced nonlinear optomechanics in a coupled-mode photonic crystal device, *Nature Communications* **14**, 1526 (2023).
- [53] J. D. Thompson, B. M. Zwickl, A. M. Jayich, F. Marquardt, S. M. Girvin, and J. G. E. Harris, Strong dispersive coupling of a high-finesse cavity to a micromechanical membrane, *Nature* **452**, 72 (2008).
- [54] A. M. Jayich, J. C. Sankey, B. M. Zwickl, C. Yang, J. D. Thompson, S. M. Girvin, A. A. Clerk, F. Marquardt, and J. G. E. Harris, Dispersive optomechanics: a membrane inside a cavity, *New Journal of Physics* **10**, 095008 (2008).
- [55] D. J. Wilson, C. A. Regal, S. B. Papp, and H. J. Kimble, Cavity Optomechanics with Stoichiometric SiN Films, *Physical Review Letters* **103**, 207204 (2009).
- [56] H. K. Cheung and C. K. Law, Nonadiabatic optomechanical Hamiltonian of a moving dielectric membrane in a cavity, *Physical Review A* **84**, 023812 (2011).
- [57] If $g < 0$ the minus sign appears outside the square root in \tilde{x}, \tilde{p} . The equations of motion (3) are invariant under $x \rightarrow -x, p \rightarrow -p$.
- [58] L. F. Buchmann, L. Zhang, A. Chiruvelli, and P. Meystre, Macroscopic Tunneling of a Membrane in an Optomechanical Double-Well Potential, *Physical Review Letters* **108**, 210403 (2012).
- [59] H. Seok, L. F. Buchmann, E. M. Wright, and P. Meystre, Multimode strong-coupling quantum optomechanics, *Physical Review A* **88**, 063850 (2013).
- [60] S. H. Strogatz, *Nonlinear dynamics and chaos: with applications to physics, biology, chemistry, and engineering*, second edition ed. (Westview Press, a member of the Perseus Books Group, Boulder, CO, 2015).
- [61] A. Wolf, J. B. Swift, H. L. Swinney, and J. A. Vastano, Determining Lyapunov exponents from a time series, *Physica D: Nonlinear Phenomena* **16**, 285 (1985).
- [62] P. Bryant, R. Brown, and H. D. I. Abarbanel, Lyapunov exponents from observed time series, *Physical Review Letters* **65**, 1523 (1990).
- [63] P. Grassberger and I. Procaccia, Measuring the strangeness of strange attractors, *Physica D: Nonlinear Phenomena* **9**, 189 (1983).
- [64] F. Elste, S. M. Girvin, and A. A. Clerk, Quantum Noise Interference and Backaction Cooling in Cavity Nanomechanics, *Physical Review Letters* **102**, 207209 (2009).
- [65] Y. Yanay, J. C. Sankey, and A. A. Clerk, Quantum backaction and noise interference in asymmetric two-cavity optomechanical systems, *Physical Review A* **93**, 063809 (2016).
- [66] C. Reinhardt, T. Müller, A. Bourassa, and J. C. Sankey, Ultralow-Noise SiN Trampoline Resonators for Sensing and Optomechanics, *Physical Review X* **6**, 021001 (2016).
- [67] P. Fonseca, E. Aranas, J. Millen, T. Monteiro, and P. Barker, Nonlinear Dynamics and Strong Cavity Cooling of Levitated Nanoparticles, *Physical Review Letters* **117**, 173602 (2016).
- [68] U. Delić, M. Reisenbauer, K. Dare, D. Grass, V. Vuletić, N. Kiesel, and M. Aspelmeyer, Cooling of a levitated nanoparticle to the motional quantum ground state, *Science* **367**, 892 (2020).
- [69] S. Leo Kingston, T. Kapitaniak, and S. K. Dana, Transition to hyperchaos: Sudden expansion of attractor and intermittent large-amplitude events in dynamical systems, *Chaos: An Interdisciplinary Journal of Nonlinear Science* **32**, 081106 (2022).
- [70] I. R. Garashchuk, D. I. Sinelshchikov, A. O. Kazakov, and N. A. Kudryashov, Hyperchaos and multistability in the model of two interacting microbubble contrast agents, *Chaos: An Interdisciplinary Journal of Nonlinear Science* **29**, 063131 (2019).
- [71] S. S. Sajjadi, D. Baleanu, A. Jajarmi, and H. M. Pirouz, A new adaptive synchronization and hyperchaos control of a biological snap oscillator, *Chaos, Solitons & Fractals* **138**, 109919 (2020).
- [72] H. Lin, C. Wang, and Y. Tan, Hidden extreme multistability with hyperchaos and transient chaos in a Hopfield neural network affected by electromagnetic radiation, *Nonlinear Dynamics* **99**, 2369 (2020).
- [73] G. Datseris and U. Parlitz, *Nonlinear dynamics: a concise introduction interlaced with code*, Undergraduate lecture notes in physics (Springer Cham, 2022).
- [74] G. Benettin, L. Galgani, A. Giorgilli, and J.-M. Strelcyn, Lyapunov Characteristic Exponents for smooth dynamical systems and for hamiltonian systems; A method for computing all of them. Part 2: Numerical application, *Meccanica* **15**, 21 (1980).
- [75] G. Benettin, L. Galgani, A. Giorgilli, and J.-M. Strelcyn, Lyapunov Characteristic Exponents for smooth dynamical systems and for hamiltonian systems; a method for computing all of them. Part 1: Theory, *Meccanica* **15**, 9 (1980).
- [76] G. Datseris, I. Kottlarz, A. P. Braun, and U. Parlitz, Estimating fractal dimensions: A comparative review and open source implementations, *Chaos: An Interdisciplinary Journal of Nonlinear Science* **33**, 102101 (2023).
- [77] K. Judd, An improved estimator of dimension and some comments on providing confidence intervals, *Physica D:*

- [Nonlinear Phenomena](#) **56**, 216 (1992).
- [78] V. Deshmukh, E. Bradley, J. Garland, and J. D. Meiss, Toward automated extraction and characterization of scaling regions in dynamical systems, [Chaos: An Interdisciplinary Journal of Nonlinear Science](#) **31**, 123102 (2021).